

LIDAR INTENSITY FOR IMPROVED DETECTION OF INUNDATION BELOW THE FOREST CANOPY

Megan W. Lang and Greg W. McCarty

USDA-ARS

Remote Sensing and Hydrology Laboratory, Beltsville Agricultural Research Center

Bldg 007, Rm 104, 10300 Baltimore Ave., Beltsville, Maryland, USA 20705

E-mail: Megan.Lang@gmail.com

Abstract: Wetland hydrology is an important factor controlling wetland function and extent, and should therefore be a vital part of any wetland mapping program. Broad-scale forested wetland hydrology has been difficult to study with conventional remote sensing methods. Airborne Light Detection and Ranging (LiDAR) is a new and rapidly developing technology. LiDAR data have mainly been used to derive information on elevation. However, the intensity (amplitude) of the signal has the potential to significantly improve the ability to remotely monitor inundation – an important component of wetland hydrology. A comparison between LiDAR intensity data collected during peak hydrologic expression and detailed *in situ* data from a series of forested wetlands on the eastern shore of Maryland demonstrate the strong potential of LiDAR intensity data for this application (> 96% overall accuracy). The relative ability of LiDAR intensity data for forest inundation mapping was compared with that of a false color near-infrared aerial photograph collected coincident with the LiDAR intensity (70% overall accuracy; currently the most commonly used method for wetland mapping) and a wetness index map derived from a digital elevation model. The potential of LiDAR intensity data is strong for addressing issues related to the regulatory status of wetlands and measuring the delivery of ecosystem services.

Key Words: forested wetlands, hydrology, inundation, wetland mapping

INTRODUCTION

Efforts are being made to conserve wetlands and many regulatory policies have been adopted in support of this goal. To manage the loss, preservation, and/or restoration of wetlands and to judge the effectiveness of these efforts in preserving associated ecosystem services, wetlands must be routinely monitored. Wetland mapping is an essential part of this monitoring program and much effort has been made by state and federal government agencies, as well as other organizations, to provide quality map products. Wetland hydrology is the most important abiotic factor controlling ecosystem function and extent (Mitsch and Gosselink 2007), and should be an important part of any wetland mapping or monitoring program.

Optical data (e.g., aerial photographs and multi-spectral images) have traditionally been used to map wetlands and information on topography has been used to supplement that approach (Lang and McCarty 2008). However, broad-scale forested wetland hydrology has been difficult to study with conventional remotely sensed methods (Tiner 1990, Lang and McCarty 2008). As a result, forested wetlands are one of the most difficult types of wetlands to map. Regardless, remote observation of

forested wetlands is necessary because they are often difficult to access on the ground, and on-site mapping at the landscape scale is usually cost prohibitive (Silva et al. 2008). New approaches are needed to map forested wetlands because they are the most common type of wetland found in the U.S. and the type of wetland most likely to be lost in the future (U.S. Fish and Wildlife Service 2002).

Light Detection and Ranging (LiDAR) is a rapidly evolving remote sensing technology, which has the potential to improve the detail and reliability of forested wetland maps and the ability to monitor parameters such as wetland hydrology (i.e., inundation; Lang and McCarty 2008). LiDARs are active sensors, sending and receiving laser energy produced by the sensor itself instead of relying on the sun's energy. This study focused on the use of discrete point return LiDAR data, which are increasingly available from state or local governments (Roger Barlow, U.S. Geological Survey, personal communication, Vierling et al. 2008), are readily available from commercial mapping companies (Rosso et al. 2006), and are most commonly used for terrestrial LiDAR mapping activities. LiDARs emit short pulses of energy and these pulses illuminate very small portions of the land's surface. Therefore,

LiDAR pulse density refers to the number of these pulses emitted by the sensor per area (i.e., pulses transmitted/m²) whereas the phrase LiDAR point density or LiDAR point cloud density is used to refer to the number of these pulses which are recorded by the sensor per area (i.e., data points/m²). A recent survey of airborne LiDAR sensors (Lemmens 2007) found that most terrestrial LiDAR sensors operate in the 900 to 1550 nm range, with 1064 nm being a very commonly used laser wavelength (Goodwin et al. 2006). LiDAR data can be used to calculate precise x,y,z locations by calculating the distance to an object by recording the amount of time it takes for an emitted pulse, or a portion of that pulse, to return to the sensor (Goodwin et al. 2006, Vierling et al. 2008). If the return signal is above a certain threshold the sensor will record it. Return intensity is largely determined by the reflective properties of materials within the light path. Signal return intensity data are commonly delivered by LiDAR providers. LiDAR intensity or amplitude is generally the amount of energy returned to the sensor per LiDAR echo relative to the amount of energy transmitted by the sensor per laser pulse (Chust et al. 2008). A digital elevation model (DEM) is the most common product derived from LiDAR data (Kaasalainen et al. 2008). A wetness index map is a secondary product, which can be generated from a DEM and is simply a function of the topographic characteristics (e.g., slope and contributing area) of the DEM (Böhner et al. 2002, Murphy et al. 2007). More information on LiDAR sensors can be found in Wehr and Lohr 1999, Flood 2001, and Goodwin et al. 2006.

Intensity data can be used to identify different types of materials on the ground, especially if those features have very distinct reflectances in the portion of the electromagnetic spectrum detected by the sensor. Due in part to the rapid development of LiDAR technology and lack of a widely accepted method to standardize LiDAR intensity data (Hyypä et al. 2008), few studies have utilized LiDAR intensity data for image classification. Most LiDAR intensity studies have focused on forestry and other types of vegetation related applications. Song et al. (2002) was one of the first studies to examine the ability of LiDAR intensity data to differentiate different materials (e.g., tree, grass, house, and asphalt road) on the ground. A few studies have used LiDAR intensity data along with other inputs to classify open water (e.g., ocean and pond; Brennan and Webster 2006, Antonarakis et al. 2008). Chust et al. (2008) and Goodale et al. (2007) used a variety of LiDAR derived products to map coastal ecosystems but only Goodale found

LiDAR intensity to be valuable. No studies have examined the ability of LiDAR intensity data to map inundation below the forest canopy, especially relatively small discontinuous areas of inundation.

With the rapid evolution of LiDAR technology, standardized procedures for handling intensity data are still lacking and methods necessary for many applications have not been fully developed (Flood 2001). However, we hypothesize that LiDAR intensity data are well suited for the identification of inundation even below the forest canopy due to the strong absorption of incident near-infrared energy (the energy detected by most terrestrial LiDAR sensors) by water and the ability to filter the data by order of return. The objective of this paper is to demonstrate the feasibility of using LiDAR intensity data to improve mapping of inundation below the forest canopy and to compare the relative ability of LiDAR intensity data for this purpose to that of optical data, currently the most commonly used method for wetland mapping.

METHODS

Study Site

The 33 km² study site is located within the headwaters of the 1756 km² Choptank River Watershed (Figure 1) which is situated on the Delmarva Peninsula within the Coastal Plain Physiographic Province. The area is characterized by a humid, temperate climate with annual precipitation of approximately 120 cm/yr on average (Ator et al. 2005). About half of annual precipitation is lost to the atmosphere via evapotranspiration while the remainder recharges ground water or enters streams via surface water. Surface water levels vary throughout the year with peak expression in early spring (March/April) while levels of evapotranspiration are still relatively low. The watershed is relatively flat (max elevation < 30 masl) and land cover is dominated by agriculture (~ 65%) with smaller amounts of forest (26%) and urban area (6%; Fisher et al. 2006). A large percent of the watershed's forests are forested wetlands. However, much of the watershed has been drained or otherwise hydrologically modified to accommodate agriculture and it is likely that the area of forested wetlands in the watershed was once much greater (Lang et al. 2008). The primary types of wetlands found within the study area are wetland depressions (e.g., Delmarva bays) and wetland flats, with smaller amounts of forested wetland area in riparian wetlands. These forested wetlands have the potential to reduce and

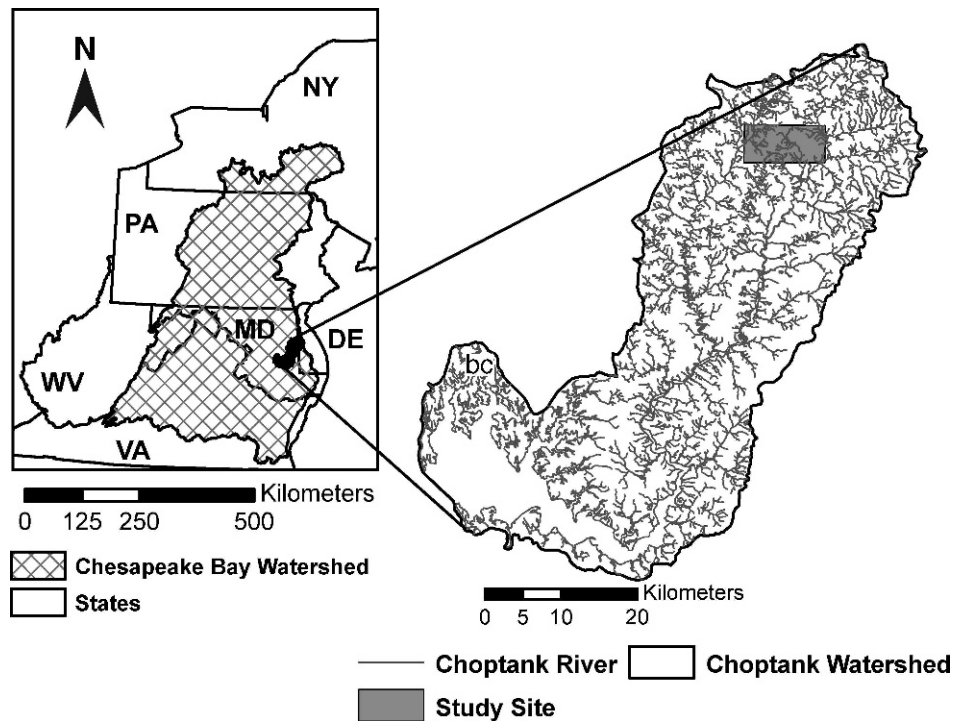


Figure 1. Map of the study site showing placement within the Choptank Watershed.

transform agrochemicals before they enter the Choptank River, a major tributary of the Chesapeake Bay.

Remotely Sensed Data

The Optech ALTM 3100 LiDAR sensor was used by the Canaan Valley Institute (Morgantown, West Virginia) on March 27, 2007 to collect data on elevation and return intensity over a 33 km² area in the headwaters of the Choptank River Watershed (Figure 1). This date corresponded with seasonally high ground water levels and an extended period of low evapotranspiration resulting in the inundation of most forested wetlands. The sensor was flown at 610 m above the Earth's surface and data were collected with a pulse frequency of 100,000 pulses of 1064 nm energy per second at a scan angle of $\pm 20^\circ$ using a scan frequency of 50 Hz. Up to 4 returns were collected (i.e., first, second, third, and last) and intensity of each return was captured with a 12 bit dynamic range. Raw data were converted to LAS files containing x, y, z, and intensity data and bare Earth points were classified by the data provider using Terrascan (Terrasolid Limited, Jyväskylä, Finland) software. LiDAR points were validated using over 100 precision GPS points collected at areas of stable elevation (e.g., road intersections) using a Trimble RTK 4700 GPS/base station

combination and a surveyed Maryland State Highway Administration benchmark. Average horizontal and vertical precision of the Trimble GPS was found to be 0.006 m (standard deviation 0.005 m) and 0.009 m (standard deviation 0.010 m), respectively. The resultant data had a vertical accuracy of ≤ 15 cm, an average bare Earth point density of ~ 2.5 pts m⁻² (~ 0.4 m post spacing), and an average point cloud density of ~ 12 pts m⁻² including all returns. The intensity data were not calibrated due to the lack of a commonly accepted LiDAR intensity calibration process and the basic information necessary to standardize the data set (e.g., range per point). It should be noted that information necessary to calibrate or standardize LiDAR intensity data is usually not provided to data users. Regardless, the influence of confounding parameters (i.e., factors other than the parameter of interest) was minimized by collecting data at a study site with minimal topographic variations, using a moderate scan angle to reduce variations due to range (Luzum et al. 2005), and collecting the data over a short time period on a day with no noticeable atmospheric interference to reduce the impact of atmospheric absorption. The ALTM 3100 sensor was coupled with a digital camera to capture coincident 12 cm spatial resolution aerial photography in the near-infrared (720–920 nm), red (600–720 nm), and green (510–600 nm) bands.

A Leica ALS50-II multiple return laser scanning system was used by Fugro EarthData on December 24, 2007 to collect a second overpass of airborne LiDAR data over the same study site. These data were collected when wetlands were not inundated to test the ability of LiDAR intensity data to detect inundation and to insure accurate vertical point measurements for the creation of a DEM. The ALS50-II sensor and the Optech ALTM 3100 sensors were similar (e.g., 4 return LiDAR sensors using 1064 nm energy). Moreover, flight and sensor parameters were modified to maximize similarities between data collections and similar efforts were made to preprocess the data and ensure data accuracy. The resultant data had a vertical accuracy of ≤ 15 cm and a pulse density of ~ 2.8 pts m^{-2} (~ 0.35 m post spacing).

Ground Data

Forested areas contained within two Nature Conservancy (TNC) reserves were visited within one week of the March LiDAR data collection to observe conditions on the ground during overflight. No significant precipitation occurred during this period. Transects were walked through forested areas collecting GPS points with a Trimble GeoXT Pocket PC approximately every 5 to 10 meters. The Trimble GeoXT GPS was designed to operate under a forest canopy and is capable of collecting data with sub-meter accuracy. GPS accuracy was enhanced by real-time WAAS correction and multiple (> 15) GPS readings were collected at each location to increase the positional accuracy of the data. The location of transects was not pre-determined and was, in part, controlled by accessibility after entering forest patches from random access points. At each stop, it was noted whether or not an area was inundated or not inundated. GPS points were collected in areas of either inundation or non-inundation, which were ≥ 4 m in diameter. A homogeneous area of this size (4 m diameter) was selected to exceed the guidelines suggested by Justice and Townshend (1981) and to allow for data filtering (smoothing). Large areas of open canopy (> 25 m in diameter) were avoided to limit the scope of the study to areas with a forest canopy, in keeping with the original project goal. Over 1,000 points were collected regardless of tree species. GPS points, along with categorical data (i.e., inundated or not inundated) and notes, were outputted to an ArcGIS shapefile to help assess the ability of the LiDAR intensity data to discriminate between inundated and non-inundated areas.

Analysis

LP360 software (QCoherent Software, LLC) was used to import the tiled bare Earth LAS files. Inverse weighted distance (IDW) interpolation was used to produce a 1 m gridded digital elevation model for the December date and intensity images for both dates (3/27/07 and 12/24/07). Similar to other interpolation methods, the use of IDW and the nature of LiDAR data can lead to local variation in values and filtering is used to suppress sudden increases or decreases in pixel values that may result from noise (Yu et al. 2002).

Before filtering the March and December 2007 intensity images, the "extract values to points" function (cubic convolution interpolation) in ArcGIS spatial analyst was used to extract an intensity value for each ground data collection point. By using cubic convolution interpolation when sampling the raster values, a weighted average of pixel values from the 16 nearest cell centers to the point location was used to compute a mean (ArcMap 9.2). The ability of the minimally processed intensity data to distinguish areas with inundation from areas without inundation was then assessed by computing the number of ground data collection areas from each hydrologic class (i.e., inundated or non-inundated) within 10 digital number (DN) intervals using the March intensity values (i.e., a frequency distribution was created). This procedure was repeated using the December LiDAR intensity data.

An iterative filtering procedure was then used to reduce noise in the March intensity image while preserving boundaries between land cover classes (e.g., inundated and non-inundated forests). The image was passed through an enhanced Lee filter (Lee 1980) 5 times with gradually increasing kernel sizes of 3 (twice), 5, 7, and 9 to reduce noise. Lee filters are often used to suppress noise that appears as image speckle. However the Lee filter also preserves image sharpness and mean value. After filtering, the "extract values to points" function in ArcGIS spatial analyst was used to sample pixel value for each ground data collection area. The ability of the filtered intensity data to distinguish areas with inundation from areas without inundation was then assessed by creating a frequency diagram.

Due to decreased overlap between intensity values of the inundated and non-inundated classes evident in the filtered data, this dataset was used to map inundated and non-inundated forests within the study area. Given the strong separation between the inundated and non-inundated forest classes, a simple threshold technique was used to produce the

classification after masking non-forested areas off using a map of forest canopy cover (Homer et al. 2004). Areas with intensity values between 0 and 50 were mapped as inundated while areas with intensity values between 80 and 255 were mapped as not inundated. The 30 DN range between the 2 classes was mapped as transition to help account for variability in intensity caused by differences in vegetation condition (e.g., evergreen and deciduous) and because areas that are not 100% inundated or not inundated are often present in the natural environment.

A map depicting evergreen forest was developed using the 3 band visible/near-infrared digital image collected coincident with the March LiDAR data (see earlier section on remotely sensed data) to help determine how large of an area and which areas may be influenced by evergreen forest canopy. The evergreen map was created by resampling the 3 band visible/near-infrared data to 1 m, using the red and near-infrared bands to produce a normalized difference vegetation index (NDVI; NIR-Red/NIR+Red; Tucker 1979), and then thresholding the NDVI so that pixels with an NDVI value of 0.08 and higher were considered to have evergreen vegetation. The threshold was set at an NDVI value of 0.08 based on visual interpretation of the full 12 cm resolution 3 band visible/near-infrared imagery. The evergreen map was then filtered using a 5×5 median filter to reduce outliers or noise. The area of evergreen canopy found within each forest class (i.e., inundated, non-inundated, and transition) was calculated by converting raster map classes to vectors and then using the intersect function in ArcMap. The same method was used to calculate the area of total forest considered to be wetland by the NWI along with the area considered to be wetland within the inundated, non-inundated, and transitional classes.

The relative utility of LiDAR intensity data for mapping inundated areas beneath the forest canopy was then compared with that of the visible/near-infrared data collected coincident with the March LiDAR data using an integrated 3 band digital camera as well as topographic information derived from the December LiDAR data. The ability of the 1 m near-infrared band of aerial photography was assessed using the same approach used to examine the unfiltered intensity values (i.e., frequency distribution). In this way, the relative abilities of bare Earth LiDAR intensity and aerial photography to map inundation could be compared using the same spatial resolution and portion of the electromagnetic spectrum. An unsupervised Isodata classification process (Duda and Hart 1973) was then used to

create a map of inundated and non-inundated forested areas using all bands of the 1 m digital aerial photography. All 30 Isodata classes were then manually combined in order to best differentiate areas that were inundated from areas that were not. A third class was necessary due to the large number of pixels corresponding with evergreen vegetation that could not be defined as inundated or not due to the obscuration of the ground by the canopy. The resultant map was filtered using a 5×5 median filter to remove numerous land cover patches of 1 or 2 pixels in size.

Since topographic wetness indices have been used to locate areas of concentrated water accumulation in the past, the ability of the LiDAR intensity derived product to identify areas of water accumulation was compared with that of a topographic wetness index. The DEM derived from the December LiDAR data was resampled to 3 m and filtered iteratively using a low pass filter to eliminate sinks (i.e., pixel(s) that were not adjacent to pixels with lower values) that do not represent overall wetness patterns (i.e., fine scale fluctuations that may be noise or a tiny depression that does not exert a significant influence on the accumulation of water) before using the data to compute a wetness index. The wetness index was calculated using SAGA version 2.0 (Cimmery 2007) according to the procedure described in (Böhner et al. 2002). The contribution of topographic information to the ability to detect inundation was determined using the frequency distribution method described above.

RESULTS

Inundated and non-inundated classes could be distinguished using the unfiltered original intensity data but a small amount of overlap between classes was evident on the frequency distribution (Figure 2). Areas identified as inundated using the ground control data had intensity values ranging from 2 to 237 (26 mean) with all but 64 (out of 658 total) having intensity values between 2 and 50. Areas identified as not inundated on the ground had intensity values ranging from 11 to 255 (175 mean) with all but 19 (out of 488 total) having intensity values between 50 and 255. After filtering, inundated and non-inundated classes were easier to distinguish because filtering reduced variability in intensity values within inundated and non-inundated classes (Figure 2). Areas identified as inundated using the ground control data had intensity values ranging from 0 to 110 (6 mean) with all but 23 (out of 658 total) inundated sites having intensity values between 0 and 50. Areas identified as not inundated on

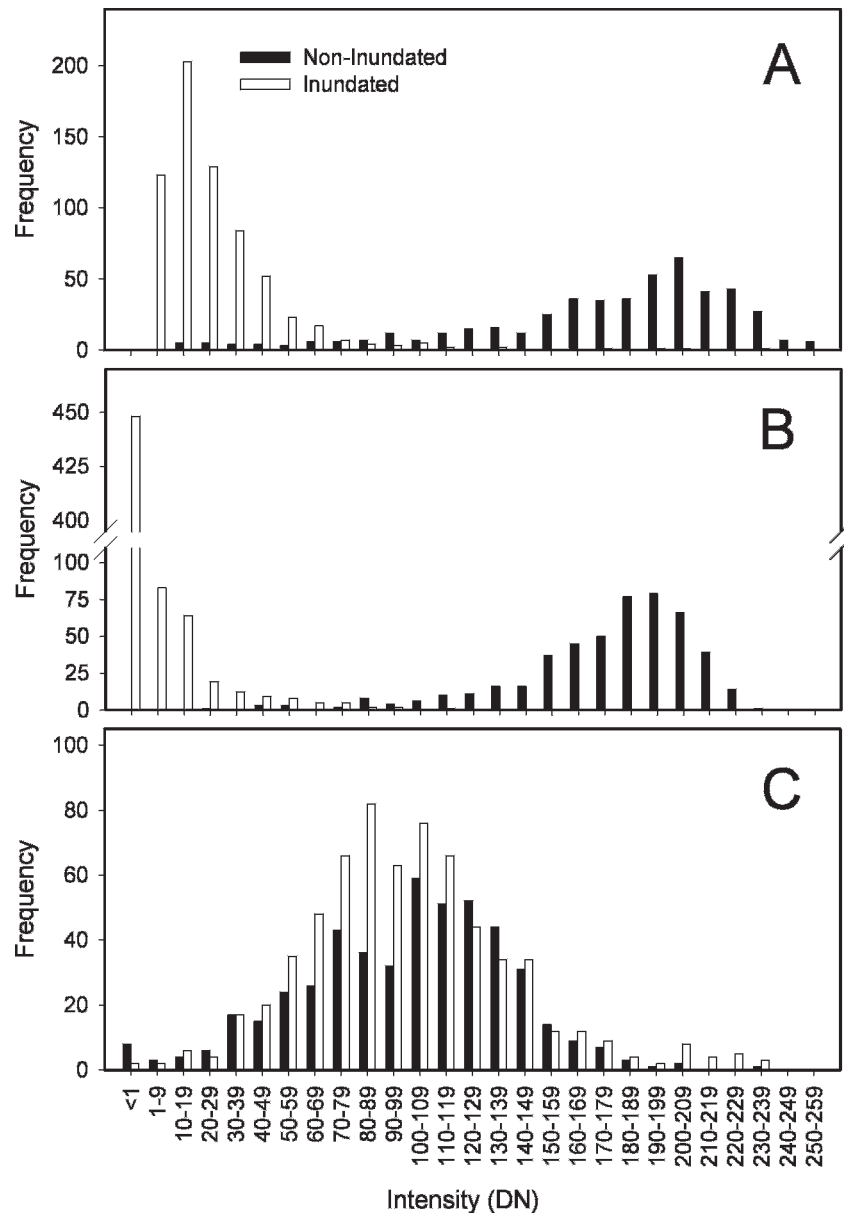


Figure 2. Frequency distributions of: A) unfiltered March LiDAR intensity data, B) filtered March LiDAR intensity data, and C) December LiDAR intensity data. All frequency distributions were created with data sampled from areas found to be inundated or non-inundated on the ground.

the ground had intensity values ranging from 27 to 237 (176 mean) with all but 4 (out of 488 total) having intensity values between 50 and 255. As expected, inundated and non-inundated classes were not easily distinguished using the December LiDAR intensity data (Figure 2). Areas identified as inundated using the ground control data had intensity values ranging from 0 to 255 (100 mean). Areas identified as not inundated on the ground had intensity values ranging from 0 to 235 (100 mean).

The filtered intensity data were able to map areas of inundation beneath the forest canopy with a high degree of accuracy (overall accuracy 96.3% when

including all transitional areas as errors; Congalton and Green 1999). Of the 658 ground data collection sites that were identified as inundated, the classification identified 636 correctly (96.7%) and none (0%) as non-inundated (22 identified as transitional areas, 3.3%). Of the 488 ground data collection sites that were identified as non-inundated, the classification identified 464 (95.1%) correctly and 4 (0.8%) as inundated (20 identified as transitional areas, 4.1%). Approximately 4% of the entire forested area had an evergreen canopy. Areas with an evergreen canopy were primarily found within the transitional class (46%), with almost as much found within the

non-inundated class (39%), and much less found within the inundated class (15%).

Near-infrared digital aerial photography collected coincident with the March LiDAR data was much less accurate in distinguishing areas of inundation below the forest canopy as compared with the LiDAR intensity data (filtered and unfiltered; Figure 3). Areas identified as inundated using ground control data had intensity values ranging from 56 to 182 (113 mean). Areas identified as not inundated on the ground had intensity values ranging from 93 to 192 (138 mean). The 3 band digital aerial photography mapped areas of inundation beneath the forest canopy with a moderate degree of accuracy (overall accuracy 70.0% including evergreen areas as errors; Congalton and Green 1999). Of the 658 ground data collection sites that were identified as inundated, the classification identified 433 correctly as inundated (65.8%) and 213 as non-inundated (32.4%; 12 [1.8%] identified as areas with an evergreen canopy; Figure 4). Of the 488 ground data collection sites that were identified as non-inundated, the classification identified 368 (75.4%) correctly as non-inundated and 82 (16.8%) as inundated (37 [7.6%] identified as evergreen). The classifications of forest inundation produced using the digital aerial photography and the LiDAR intensity data generally identified the same areas as inundated (Figure 5). However, the map produced using the near-infrared digital aerial photography was much grainier and boundaries between classes were less distinct even after the classification was filtered.

Approximately 53% of the total forested area found within the study area was categorized as wetland by NWI. Of that 8.30 km² area, 65% (5.37 km²) was deemed to be non-inundated by the filtered intensity based map, 18% (1.50 km²) to be inundated, and 17% (1.42 km²) to be transitional. Significant areas of forest that were mapped as wetland by NWI did not appear to be wetlands on the digital aerial photography. However, ditches were found in some of these areas (Figure 6).

Although similarities were found between the forest inundation map produced using the March LiDAR intensity data and the wetness index produced using the DEM (Figure 6), the wetness index was less able to distinguish inundated from non-inundated areas (Figure 3). The inundated areas were generally found to have higher wetness index values and the non-inundated areas were generally found to have lower wetness index values but there was a large amount of overlap between inundated ground data collection areas having wetness index values between 7.58 and 13.27 (mean

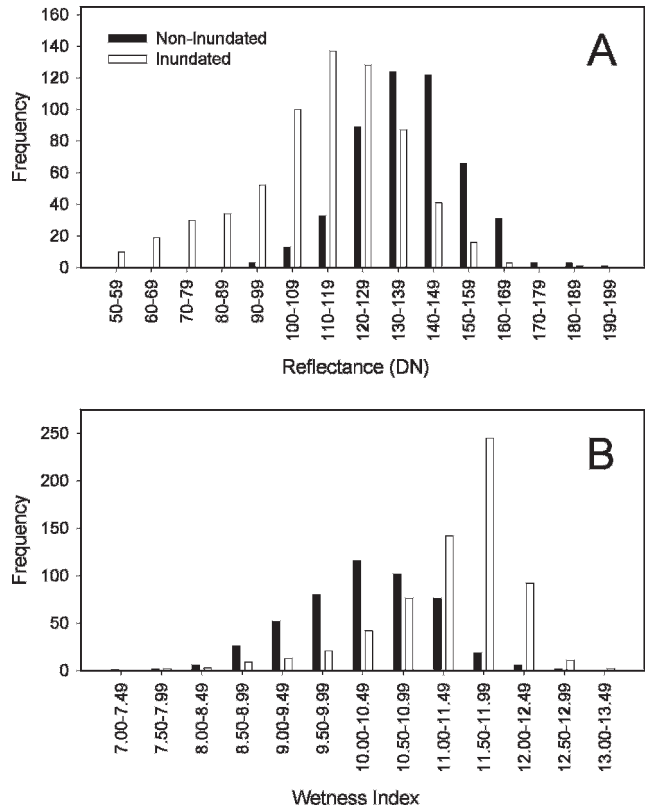


Figure 3. Frequency distributions of: A) 1 m near-infrared digital aerial photography data and B) wetness index values which were computed using the December digital elevation model. Both frequency distributions were created with data sampled from areas found to be inundated or non-inundated on the ground.

11.34) and the non-inundated ground data collection points having wetness index values between 7.33 and 12.78 (mean 10.28).

DISCUSSION

Enhanced Lee filtering was found to increase the ability of LiDAR intensity data to distinguish between areas with and without inundation (Figure 2). The use of this filter changed the mean of non-inundated areas by only 1 DN but it decreased average DN in inundated areas by 20, which was unexpected as enhanced Lee filtering does not normally alter the mean. Filtering resulted in the concentration of intensity values near class means, reducing the range over which values were spread. This may be due to the ability of filtering to reduce noise (Song et al. 2002, Chust et al. 2008) thus improving signal to noise ratio. When considering LiDAR intensity data, there are multiple sources of the noise. The salt and pepper appearance (speckle) of unfiltered intensity image can be at least partially attributable to sensor error (Song et al. 2002, Yu et

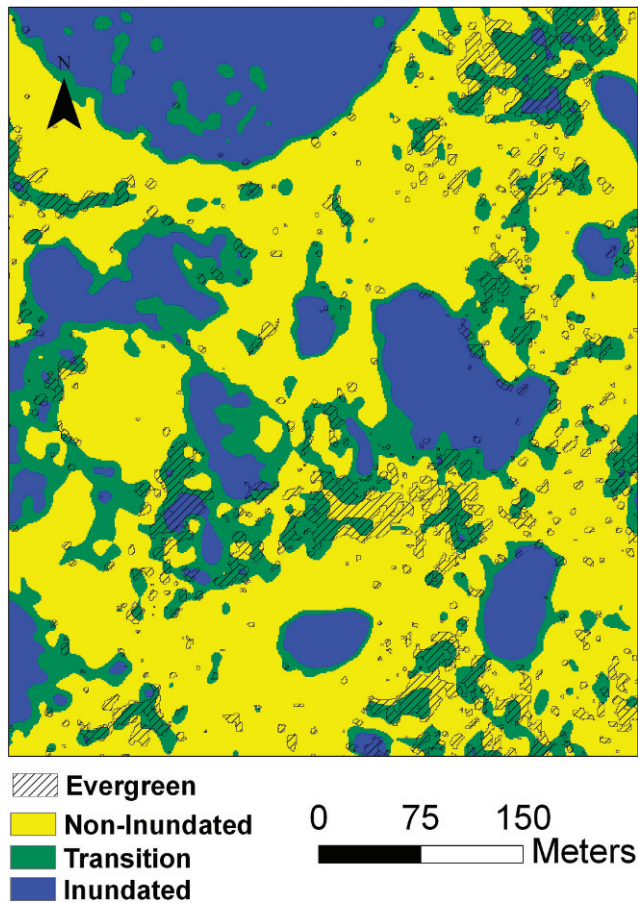


Figure 4. Forest inundation map derived from the March LiDAR data overlain with polygons representing areas of evergreen forest produced using the aerial photographs collected coincident with the March LiDAR data.

al. 2002, Chust et al. 2008) and to the irregular orientation of objects (e.g., tree trunks or hummocks) below the canopy leading to variations in local incidence angles and thus varying degrees of energy being returned to the sensor. Other studies confirm that the use of filtering improves land cover classification (Song et al. 2002, Chust et al. 2008).

The forest inundation classification identified areas of inundation with a high degree of accuracy ($\sim 96.7\%$), which should be acceptable for most natural resource applications. Antonarakis et al. (2008) achieved similar accuracies (95–99% accuracy) when classifying open water (i.e., a river) using a combination of LiDAR intensity and LiDAR derived elevation metrics. The sensitivity of the March intensity image to inundation was further supported by the lack of apparent inundation features on the December image (Figure 7). The accuracy of the intensity derived forest inundation map was bolstered by focusing the analysis on the feature of interest (i.e., ground below the forest

canopy) through the use of a forest mask and filtering the LiDAR returns by elevation.

The small amount of classification error identified in the LiDAR derived forest inundation map can be attributed to both ground and sensor characteristics. It is probable that the presence of an evergreen canopy caused a slight decrease ($\leq \sim 3.3\%$) in the accuracy of the map. The majority of areas with an evergreen canopy (46%) corresponded with the transitional class on the forest inundation map. These transitional areas had intensity values that were higher than most areas of inundation but lower than most areas without inundation. Although this may have been caused by mixed (inundated and not inundated) pixels due to GPS error or differences in soil moisture (Goodale et al. 2007, Antonarakis et al. 2008), it could also have been caused by the lower intensity of ground returns beneath evergreen canopy. This reduction in signal could be caused by a variety of factors including reduced transmittance of energy through the forest canopy or reduced sensitivity of the sensor to the returned energy as controlled by gain, the first explanation being more probable. Figure 4 illustrates a portion of the classification with a relatively large area of evergreen vegetation. Note that there is some correspondence between areas designated as transitional and areas with an evergreen canopy. The study area had a relatively small area of evergreen forest (4%), primarily as American holly (*Ilex opaca* Aiton) and mixed pines (e.g., *Pinus taeda* L. and *Pinus virginiana* Mill.). Forested wetlands are one of the most difficult classes of wetlands to detect and evergreen forested wetlands are one of the most difficult types of forested wetlands to detect using optical data. Therefore a slight reduction in classification accuracy due to the presence of evergreen vegetation was expected and is a relative improvement upon the ability to map evergreen forested wetlands. In addition to fine scale variability in intensity (i.e., speckle), overall variations in intensity within the inundated class may be caused by differences in scan angle across flight lines (Kaasalainen et al. 2005, Luzum et al. 2005). Variability due to variations in vegetation structure and local incidence angle (a combination of sensor scan angle and the orientation of objects on the ground) dominates in rougher surfaces, such as upland forests (Kaasalainen et al. 2005).

Even when using the same portion of the electromagnetic spectrum and an identical spatial resolution (1 m), the LiDAR intensity data (filtered and unfiltered) was much more capable of distinguishing inundated from non-inundated areas below the forest canopy than the near-infrared optical

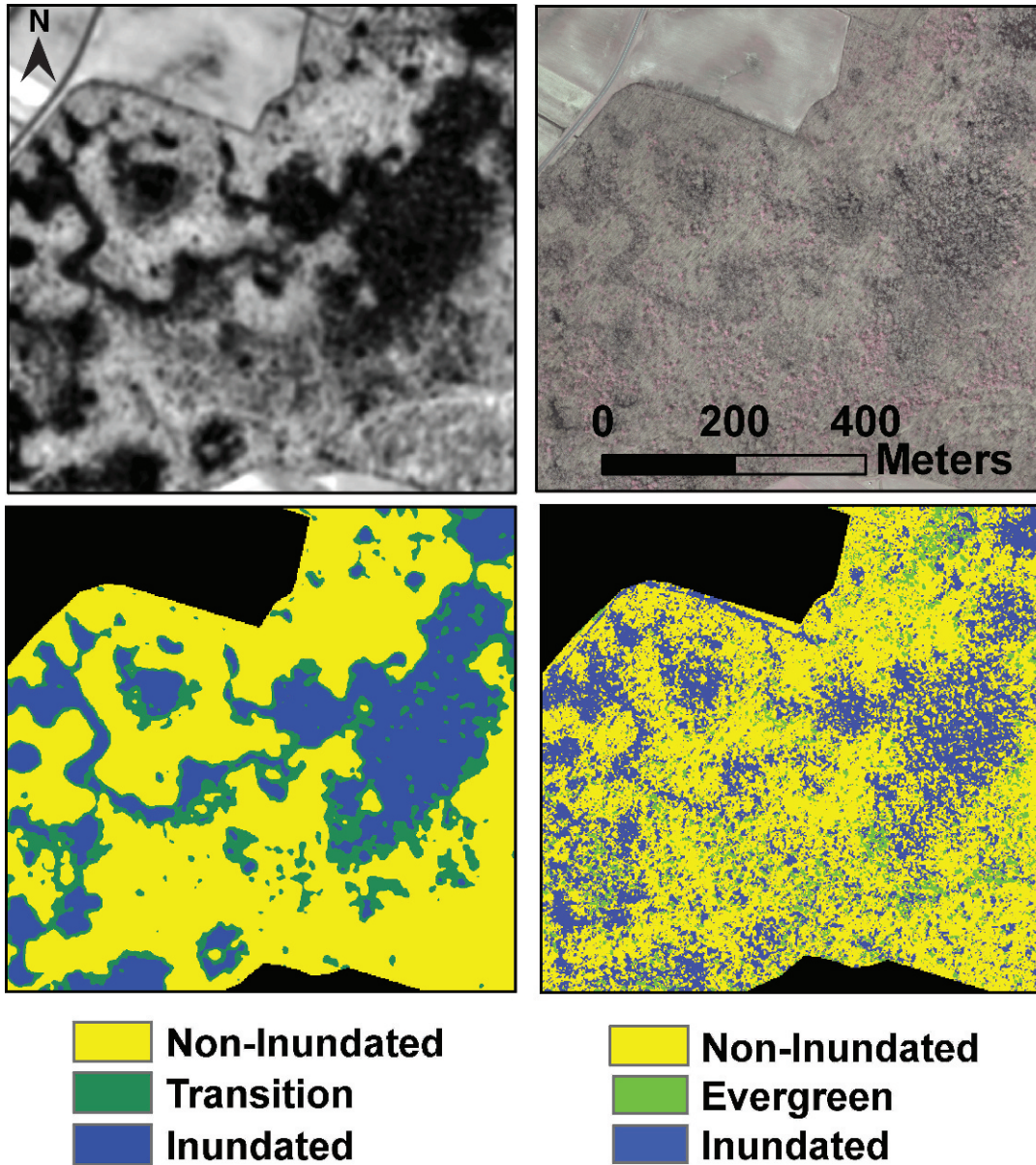


Figure 5. The original datasets (filtered intensity, above left and aerial photography, above right) used to produce two different forest inundation maps (resultant map directly below parent data set).

band. This is evident in the frequency distributions of the intensity and optical data (Figures 2 and 3). The frequency distribution based on optical data shows a much greater number of pixels with values that could belong to areas with or without inundation, as compared with the LiDAR intensity based frequency distributions. Figure 5 illustrates that although the general placement of inundated areas is evident with both types of data, boundaries between classes and total area of inundation are much clearer when examining the intensity data.

Although it is informative to directly compare LiDAR and optical imagery collected using the same portion of the electromagnetic spectrum,

wetlands are traditionally mapped using all available bands of digital aerial photography. For this reason, the LiDAR based inundation map was also compared with a map produced using all 3 bands of the visible/near-infrared aerial photography collected coincident with the March LiDAR imagery. The forest inundation map derived from the digital aerial photography was significantly less accurate (65.8% of inundated areas identified correctly) than the forest inundation map derived from the filtered LiDAR intensity data (96.7% of inundated areas identified correctly). Evergreen areas had a significant impact on the ability of the optical data to correctly identify areas of inundation below the

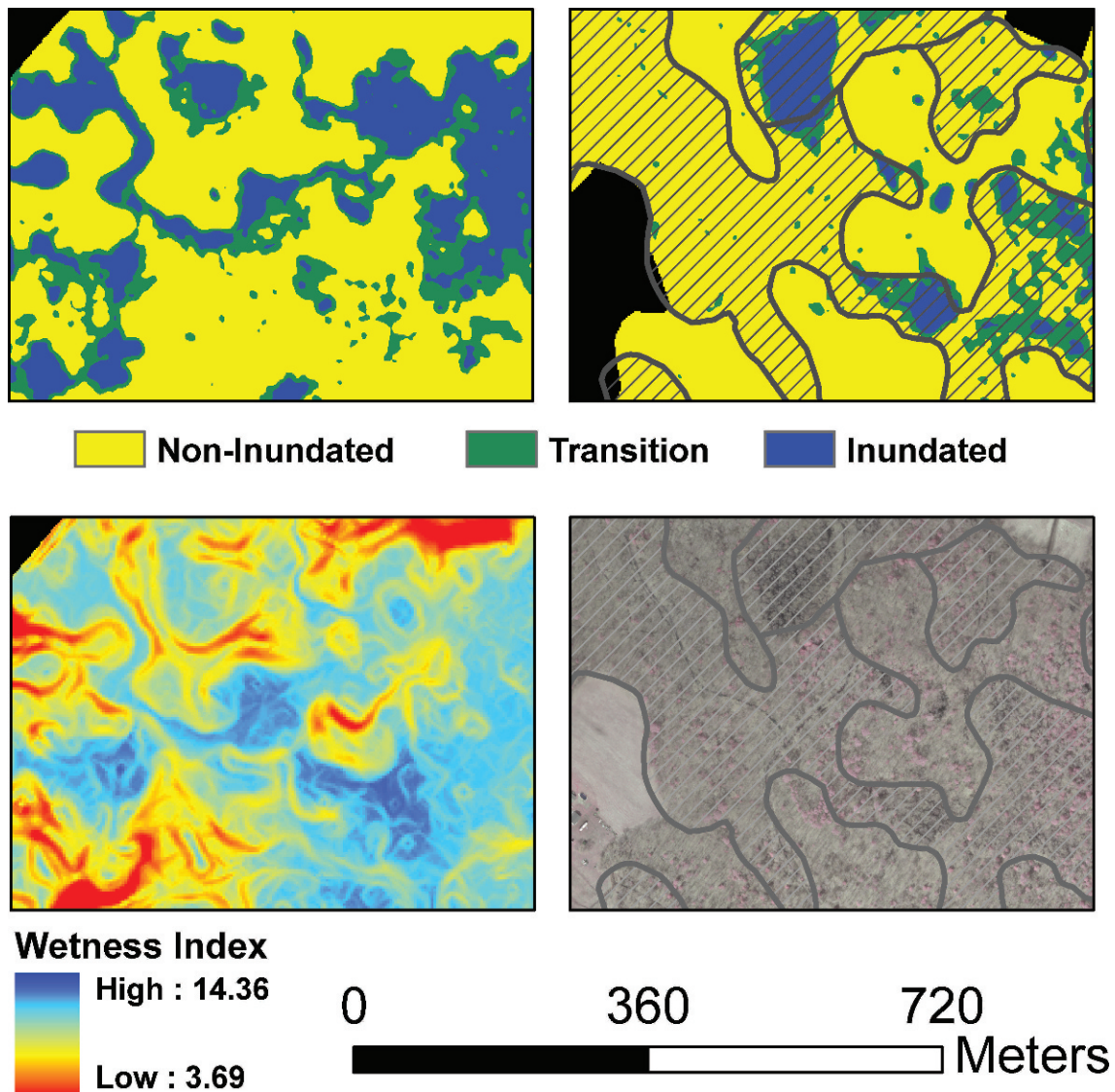


Figure 6. Forest inundation map derived from filtered LiDAR intensity data (top, right) and false color near-infrared digital aerial photograph of the same area (bottom, right). Wetlands as mapped by NWI are displayed on both images. Forest inundation map derived from filtered March LiDAR intensity data (top, left) and wetness index derived from digital elevation model for the same area (below, left). Note that many of the areas mapped as inundated on the forest inundation map (top, left) have high wetness index values (below, left).

forest canopy; 1.8% of inundated validation sites and 7.6% of non-inundated validation sites were identified as evergreen for a total of 9.4% of validation sites where ground conditions could not be identified due to the presence of evergreen vegetation. However, the presence of the leaf-off deciduous forest canopy likely had a greater impact on the ability of the optical data to identify inundated areas. The optical data identified 32.4% of inundated validation sites as non-inundated and 16.8% of non-inundated sites as inundated. Two primary causes of this misclassification were mixed pixels and shadow. Since water is a strong absorber in the green, red, and near-infrared portions of the

electromagnetic spectrum, pixels with a lower reflectance are generally categorized as inundated while those with a higher reflectance are categorized as non-inundated (Antonarakis et al. 2008). The reflectance recorded at a significant percent of inundated validation sites was likely increased due to the relatively high reflectance of tree branches and boles. Conversely, reflectance of the 16.8% of non-inundated validation sites that were classified as inundated may have been lowered by shadow. Unlike optical data, LiDAR intensity is not affected by shadow (Donoghue et al. 2007; i.e., the reduction of the sun's energy by features blocking its pathway), which often complicates the use of optical

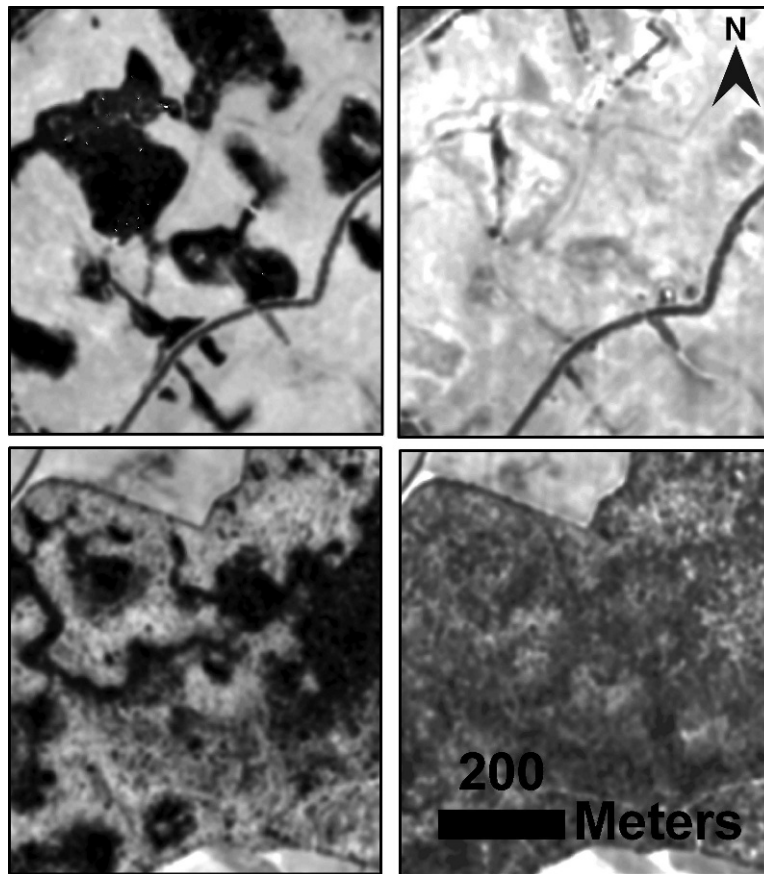


Figure 7. Filtered LiDAR intensity collected when most wetlands were inundated (left, top and bottom) and non-inundated (right, top and bottom). Images on top were collected over the same area of herbaceous restored wetlands and the images on the bottom were collected from the same area of forested wetlands.

data. We concluded that the combined influence of mixed pixels due to reflectance from tree branches and boles and shadows contributed to the finer scale texture (likely misclassifications; Figure 5) present in the forest inundation map derived from the optical data. Land cover patches in the intensity derived map were more contiguous. However, some small to medium scale patches were present in both maps and are likely due to hummocks and very small depressional wetlands (< 10 m).

NWI mapped over half of the forested area within the study site as wetlands, which is not surprising since many of the forested areas in the Choptank Watershed remain forested because they are unsuitable for farming or development due to their relatively high water levels. What was surprising was finding that 82% of the area mapped as wetland by NWI was not mapped as inundated using the March LiDAR intensity data. Generally, NWI maps error more by omission than commission, especially in forested wetlands (Tiner 1990). Estimates of the extent of NWI's forested wetland omission errors vary widely but can be substantial (Stolt and Baker

1995, Rolband 1995, Kudray and Gale 2000, Wright and Gallant 2007). Although not all wetlands are inundated and instead simply exhibit saturation in the root zone for a significant portion of the growing season, the LiDAR data were collected during a time of year when wetlands often exhibit high water levels during periods of average to above average precipitation, like the spring of 2007. Figure 6 illustrates large variation in spatial agreement between the LiDAR derived forest inundation map and the NWI wetland polygons. It is possible that areas of disagreement were caused by the draining of wetlands between the date when the NWI map was created (early 1980s) and 2007. Multiple ditches traverse the western portion of this site (see aerial photography in Figure 6). Although the minimum mapping unit is greater for NWI and this factor may be partially responsible for the overall variation between NWI and the LiDAR product, this does not appear to have caused the discrepancy illustrated in Figure 6.

Although the wetness index resulted in values between 7.33 and 13.27 and a higher average wetness

index value was found, as expected, among inundated validation areas, means of inundated and non-inundated validation areas varied by only 1.06 and the frequency diagram indicated a poor potential for discriminating areas of inundation from areas without inundation. Regardless, the map of wetness index values provides an additional source of information that could be used by natural resource managers to identify areas with a high likelihood of inundation based purely on topographic position (i.e., slope and contributing area) and areas that were likely inundated in the past (drained wetlands). Areas that are not shown to be inundated on the intensity derived forest inundation maps, but have a high wetness index, are potential candidates for wetland hydrologic restoration.

LiDAR intensity is often considered to be analogous to optical reflectance; however, because there are distinct differences between LiDAR intensity and optical reflectance, LiDAR data are not directly comparable to reflectance data obtained from optical sensors. Multiple factors, other than the reflectance of the material on the ground, can influence the intensity of the LiDAR return (Goodwin et al. 2006, Donoghue et al. 2007). Regardless, the potential of these data to address fundamental ecosystem processes and improve land cover classification is strong (Donoghue et al. 2007). This is especially true when attempting to differentiate classes with very distinct reflectances in the portion of the electromagnetic spectrum utilized by the sensor (e.g., water, dry leaves, soil, vegetation). Furthermore, assuming that atmospheric conditions are relatively constant during acquisition, LiDAR intensity will depend primarily on the reflectance of objects on the ground at the wavelength of the laser (Luzum et al. 2005) and other properties of the material being sensed. The influence of confounding parameters can be greatly reduced by optimizing collection parameters to reduce noise, such as in this study and others (Holmgren and Persson 2004, Donoghue et al. 2007).

The increasing availability of LiDAR sensors that use various wavelength lasers and other instrument specifications (e.g., pulse repetition rate; Lemmens 2007, Hyyppä et al. 2008) means that proper instrument selection will be increasingly important to wetland monitoring. The relationship between laser wavelength and the absorption features of water and other materials should be considered. If possible, LiDAR data should be collected to different specifications based on their application. For example, higher point densities and collection of data at lower altitudes may be necessary for mapping in forested areas with relatively subtle

topographic change (Luzum et al. 2005, Goodwin et al. 2006). Temporal considerations (e.g., date of acquisition) are also important. For example, it was necessary to collect the March dataset so that inundation could be assessed but these data could not be used to create an accurate DEM because the presence of water precludes accurate detection of the land surface.

The full potential of LiDAR technology has not been realized, in part due to the low utilization of certain LiDAR products, such as LiDAR intensity data. This is largely due to the sparse documentation of the potential of this unique product to help solve some of our most intractable natural resource problems, such as the mapping of forested wetlands. LiDAR derived forest inundation maps can be used to guide numerous management and regulatory decisions. For example, LiDAR data can be used to map hydrologic flow pathways, which regulate the ability of wetlands to provide ecosystem services (e.g., water quality). The ability to identify these hydrologic connections could be key to the preservation of many forested wetlands. Recent federal court case rulings incorporating the “significant nexus” concept in the jurisdiction of the Clean Water Act for wetland regulation have presented additional information requirements for establishing regulatory status. New tools that can establish connectivity between wetlands and stream networks would better inform debates and enhance the ability to preserve wetlands under current laws (Kusler et al. 2007).

ACKNOWLEDGMENTS

This research was supported by the U.S. Department of Agriculture Natural Resources Conservation Service Wetland Conservation Effects Assessment Project. We thank the Canaan Valley Institute for supplying the March 2007 LiDAR dataset and John Schmidt and Ravi Sripada for helping to coordinate the March 2007 acquisition. We also thank Fugro Earth Data for customer support. Most of all thanks goes to Robert Oesterling and Andrew Russ for geospatial technical support. All trade names are included for the benefit of the reader and do not imply an endorsement of or preference for the product listed by the U.S. Department of Agriculture.

LITERATURE CITED

- Antonarakis, A. S., K. S. Richards, and J. Brasington. 2008. Object-based land cover classification using airborne LiDAR. *Remote Sensing of Environment* 112:2988–98.

- Ator, S. W., J. M. Denver, D. E. Krantz, W. L. Neweell, and S. K. Martucci. 2005. A surficial hydrogeologic framework for the mid-Atlantic Coastal Plain. USGS Professional Paper, Reston, VA, USA, 1680:1-44.
- Böhner, J., R. Koethe, O. Conrad, J. Gross, A. Ringeler, and T. Selige. 2002. Soil regionalisation by means of terrain analysis and process parameterisation. p. 213-22. *In* E. Micheli, F. Nachtergaele, and L. Montanarella (eds.) Soil Classification 2001. European Soil Bureau, Luxembourg, Research Report No. 7, EUR 20398.
- Brennan, R. and T. L. Webster. 2006. Object-oriented land cover classification of LIDAR-derived surfaces. *Canadian Journal of Remote Sensing* 32:162-72.
- Chust, G., I. Galparsoro, A. Borja, J. Franco, and A. Uriarte. 2008. Coastal and estuarine habitat mapping, using LIDAR height and intensity and multi-spectral imagery. *Estuarine, Coastal and Shelf Science* 78:633-43.
- Cimmery, V. 2007. User guide for SAGA (version 2.0). <http://www.saga-gis.org/en/about/references.html>
- Congalton, R. G. and Green, K. 1999. *Assessing the Accuracy of Remotely Sensed Data: Principles and Practices*. CRC Press, Boca Raton, FL, USA.
- Donoghue, D. N. M., P. J. Watt, N. J. Cox, and J. Wilson. 2007. Remote sensing of species mixtures in conifer plantations using LiDAR height and intensity data. *Remote Sensing of Environment* 110:509-22.
- Duda, O. and P. E. Hart. 1973. *Pattern Classification and Scene Analysis*. John Wiley and Sons, Inc., New York, NY, USA.
- Fisher, T., J. Benitez, K. Lee, and A. Sutton. 2006. History of land cover change and biogeochemical impacts in the Choptank river basin in the mid-Atlantic region of the US. *International Journal of Remote Sensing* 27:3683-703.
- Flood, M. 2001. Laser altimetry: from science to commercial LIDAR mapping. *Photogrammetric Engineering and Remote Sensing* 67:1209-27.
- Goodale, R., C. Hopkinson, D. Colville, and D. Amirault-Langlais. 2007. Mapping piping plover (*Charadrius melodus melodus*) habitat in coastal areas using airborne lidar data. *Canadian Journal of Remote Sensing* 33:519-33.
- Goodwin, N. R., N. C. Coops, and D. S. Culvenor. 2006. Assessment of forest structure with airborne LiDAR and the effects of platform altitude. *Remote Sensing of Environment* 103:140-52.
- Holmgren, J. and Å. Persson. 2004. Identifying species of individual trees using airborne laser scanner. *Remote Sensing of Environment* 90:415-23.
- Homer, C., C. Huang, L. Yang, B. Wylie, and M. Coan. 2004. Development of a 2001 National Landcover Database for the United States. *Photogrammetric Engineering and Remote Sensing* 70:829-40.
- Hyyppä, J., H. Hyyppä, D. Leckie, F. Gougeon, X. Yu, and M. Maltamo. 2008. Review of methods of small-footprint airborne laser scanning for extracting forest inventory data in boreal forests. *International Journal of Remote Sensing* 29:1339-66.
- Justice, C. O. and J. R. G. Townshend. 1981. Integrating ground data with remote sensing. p. 38-58. *In* J. R. G. Townshend (ed.) *Terrain Analysis and Remote Sensing*. Allen and Unwin, London, UK.
- Kaasalainen, S., E. Ahokas, J. Hyyppä, and J. Suomalainen. 2005. Study of surface brightness from backscattered laser intensity: calibration of laser data. *IEEE Geoscience and Remote Sensing Letters* 2:255-59.
- Kaasalainen, S., A. Kukko, T. Lindroos, P. Litkey, H. Kaartinen, J. Hyyppä, and E. Ahokas. 2008. Brightness measurements and calibration with airborne and terrestrial laser scanners. *IEEE Transactions on Geoscience and Remote Sensing* 46:528-34.
- Kudray, G. M. and M. R. Gale. 2000. Evaluation of national wetland inventory maps in a heavily forested region in the upper great lakes. *Wetlands* 20:581-87.
- Kusler, J., P. Parenteau, and E. A. Thomas. 2007. "Significant nexus" and Clean Water Act jurisdiction. Association of State Wetland Managers, http://www.aswm.org/fwp/significant_nexus_paper_030507.pdf
- Lang, M. and G. McCarty. 2008. Wetland Mapping: History and Trends. p. 74-112. *In* R. E. Russo (ed.) *Wetlands: Ecology, Conservation and Management*. Nova Publishers, New York, NY, USA.
- Lang, M., G. McCarty, J. Ritchie, A. Sadeghi, D. Hively, and D. Eckles. 2008. Radar monitoring of wetland hydrology: dynamic information for the assessment of ecosystem services. *Proceedings of the 2008 IEEE International Geoscience & Remote Sensing Symposium*, Boston, MA, USA.
- Lee, J. S. 1980. Digital image enhancement and noise filtering by use of the local statistics. *IEEE Transactions on Pattern Analysis and Machine Intelligence* 2:165-168.
- Lemmens, M. 2007. Airborne lidar sensors. *GIM International* 21(2):24-27.
- Luzum, B. J., K. C. Slatton, and R. L. Shrestha. 2005. Analysis of spatial and temporal stability of airborne laser swath mapping data in feature space. *IEEE Transactions on Geoscience and Remote Sensing* 43:1403-20.
- Luzum, B., M. Starek, and K. C. Slatton. 2004. Normalizing ALSM Intensities. *Geosensing Engineering and Mapping (GEM) Civil and Coastal Engineering Department, University of Florida, USA. GEM Center Report No. Rep_2004-07-001*.
- Mitsch, W. J. and J. G. Gosselink. 2007. *Wetlands*, fourth edition. John Wiley and Sons, Inc., New York, NY, USA.
- Murphy, P. N. C., J. Ogilvie, K. Connor, and P. A. Arp. 2007. Mapping wetlands: a comparison of two different approaches for New Brunswick, Canada. *Wetlands* 27:845-54.
- Rolband, M. S. 1995. A comparison of wetland areas in northern Virginia: National wetland inventory maps versus field delineated wetlands under the 1987 manual. *Wetland Journal: Research, Restoration, Education* 7:10-14.
- Rosso, P. H., S. L. Ustin, and A. Hastings. 2006. Use of lidar to study changes associated with *Spartina* invasion in San Francisco Bay marshes. *Remote Sensing of Environment* 100:295-306.
- Silva, T. S. F., M. P. F. Costa, J. M. Melack, and E. M. L. M. Novo. 2008. Remote sensing of aquatic vegetation: theory and applications. *Environmental Monitoring and Assessment* 140:131-45.
- Song, J. H., S. H. Han, K. Y. Yong, and Y. I. Kim. 2002. Assessing the possibility of land-cover classification using LiDAR intensity data. *International Archives of Photogrammetry, Remote Sensing and Spatial Information Sciences* 34:259-62.
- Stolt, M. H. and J. C. Baker. 1995. Evaluation of National Wetland Inventory maps to inventory wetlands in the southern Blue Ridge of Virginia. *Wetlands* 15:346-53.
- Tiner, R. W. 1990. Use of high-altitude aerial photography for inventorying forested wetlands in the United States. *Forest Ecology and Management* 33:593-604.
- Tucker, C. J. 1979. Red and photographic infrared linear combinations for monitoring vegetation. *Remote Sensing of Environment* 8:127-50.
- U.S. Fish and Wildlife Service. 2002. National wetlands inventory: A strategy for the 21st century. US Department of the Interior, Fish and Wildlife Service, Washington, DC, USA.
- Vierling, K., L. Vierling, W. Gould, S. Martinuzzi, and R. Clawges. 2008. Lidar: shedding new light on habitat characterization and modeling. *Frontiers in Ecology and the Environment* 6:90-98.
- Wehr, A. and U. Lohr. 1999. Airborne laser scanning - an introduction and overview. *ISPRS Journal of Photogrammetry & Remote Sensing* 54:68-82.
- Wright, C. and A. Gallant. 2007. Improved wetland remote sensing in Yellowstone National Park using classification trees to combine TM imagery and ancillary environmental data. *Remote Sensing of Environment* 107:582-605.
- Yu, K., S. H. Han, H. Chang, and T. Ha. 2002. Potential of reflected intensity of airborne laser scanning systems in roadway features identification. *Geomatica* 56:363-74.